A Chaotic Feature Extraction Based on SMMF and CMMFD for Early Fault Diagnosis of Rolling Bearing

XIAOLI YAN, GUIJI TANG, AND XIAOLONG WANG
Department of Mechanical Engineering, North China Electric Power University, Baoding 071003, China

Corresponding author: Guiji Tang (tanggjlk@ncepu.edu.cn)

ABSTRACT Various failure mechanisms of rolling bearing under different working conditions involve important nonlinear dynamic characteristics. And the incipient fault detection of the complex and non-stationary rolling bearing signal is difficult, especially with multiple interference source components. To address this issue, a novel fault feature extraction method which integrates chaos theory and mathematical morphology is proposed. Firstly, the smooth multi-scale morphological filtering (SMMF) is adopted to reduce the noise in chaotic rolling bearing signals without destroying its original nonlinear dynamic structure. In addition, a method of generalized estimation of morphological fractal dimension called composite multi-scale morphological fractal dimension (CMMFD) is proposed, and applied to quantify the complexity of those orbits reconstructed from rolling bearing signals. The CMMFD improves the identification ability of the original morphological fractal dimension (MFD). Then, CMMFD features are extracted from SMMF denoised signal. Different conditions of rolling bearing signals are distinguished in this feature space. Finally, the CMMFD features are input into a Hidden Markov Model (HMM) training and diagnosis to distinguish different faults of rolling bearing signals. The new diagnosis approach based on SMMF and CMMFD is compared with some existing methods in analysis of simulated signals and experimental rolling bearing signals. Accuracy and efficiency of different approaches are contrasted by analyzing the results of simulation and experiments. Comparative results demonstrate that the proposed diagnosis approach based on SMMF and CMMFD can reliably recognize different fault types at the early stage and have more accurate results.

INDEX TERMS Composite multi-scale morphological fractal dimension, smooth multi-scale morphological filtering, rolling bearing, fault feature extraction.

I. INTRODUCTION

Rolling bearing is a hinge part of the mechanical transmission system, which is wide-ranging in industry. Most of the rolling bearing failure that caused equipment outage or major accidents were not detected in the early stage [1]. Therefore, early fault detection of rolling bearing is valuable for preventing equipment failure caused by its gradual evolution into a serious fault [2]. Vibration analysis is the most commonly utilized non-destructive detecting method for rotating machinery failure [3]. The incipient fault detection of the bearing signal using vibration analysis technique is respected

The associate editor coordinating the review of this manuscript and approving it for publication was Donato Impedovo.

by many researchers owing to the advantages of improved fitness and efficiency [4], [5].

The faulty rolling bearing system is categorized a into nonlinear vibration system. The nonlinear characteristics caused by wear, crack, rupture, and plastic deformation failure can exhibit rich, dynamic behavior, including sub-harmonics and super-harmonics, quasi-periodic, chaotic vibration [10]. The traditional time-domain analysis and frequency-domain analysis techniques were successfully devoted to stationary and linear signals with periodic phenomenon. But the vibration data collected from the mechanical device is complicated, non-stationary, and nonlinear. Time-domain analysis or frequency-domain analysis alone can not show detailed information from complex fault signals. Time-frequency

analysis feature techniques [6]–[9], which are more capable of simultaneously extracting detailed time-varying frequency contents from rolling bearing signals. However, the non-stationarity and nonlinearity of the fault signals are weakened to some degree by the aforementioned methods. Therefore, it is requested to research efficient methods for extracting novel fault features of signals based on nonlinear dynamics. Vibration features based on chaos theory such as the Lyapunov exponent, the entropy, and the fractal dimension are able to quantify the strange attractor characteristics of different rolling bearing healthy/faulty conditions. Nonetheless, a single-scale feature is not enough to represent all information of nonlinear signal. The division of fault state space may overlap if the feature values of two fault signals are close. Hence, it is necessary to analyze the signal with composite, multi-scale techniques to provide more comprehensive signal information for fault diagnosis.

On the other hand, the vibration signal is inevitably polluted by noise in the process of acquisition and transmission. The chaotic dynamic characteristics contained in the data may be masked by the interference of noise. And the attractor with disordered and irregular orbits means that the signal of the nonlinear dynamical system is contaminated by noise. On the contrary, the attractor with legible orbits means that the nonlinear dynamical structures of the system are not damaged. Which is useful to acquire nonlinear features effectively. Hence, effective noise suppression is often the premise of a vibration signal analysis. Conventional methods of noise reduction such as linear low-pass filtering do not work well for chaotic data since the signal and the noise often have overlapping bandwidths [11]. A few researchers have been trying to deal with noise reduction of chaotic signals by using various nonlinear methods [12]–[14]. Denoising technology of chaotic signals has been used extensively in other fields such as information systems and physiological systems. But there are few papers in literature that have discussed the noise reduction of chaotic mechanical vibration signals so far.

Mathematical morphology (MM) is an effective nonlinear analysis technique, which is different from these regular time-frequency signal analysis techniques. It can be applied to make translation matching and local correction of signal from front to back by a certain structural element (SE) [15]. Typical morphological filter (MF) uses a single-scale to analyze the signal [16]. Nevertheless, the effect of MF for noise suppression is unapparent when the scale of SE is relatively small. Conversely, the effect of MF for suppressing the noise is obvious when the scale of SE is overly large, but the detailed information of the clean signal can not be preserved well, and the waveform of the filtered signal has serious distortion. For complex signals like rolling bearing fault signals, MF with single-scale SE has limited accuracy in preserving the detailed characteristics of the original signal while suppressing noise [17]. Thus, the multi-scale morphological filtering (MMF) [18] was put forward to analyze signal at multiple scales. The effect on the MMF analysis of rolling

bearing signal gains an advantage over that of single-scale MF [19].

The application of MMF in processing the rolling bearing signals for fault diagnosis is able to be divided into two categories: Suppressing the noise and fault feature. One category is using the MMF technology to reduce the noise of vibration signals and enhance fault features of signals. Zhang *et al.* [19] introduced the average MMF analysis in recovering impulsive features from the one-dimensional rolling bearing signal contaminated by strong noise. And afterwards, the MMF has been widely used for reducing noise and enhancing features of rolling bearing fault signal. Dong *et al.* [20], Raj *et al.* [21], and Li *et al.* [22] respectively used maximum signal-to-noise ratio (SNR), maximum kurtosis, and maximum spectral kurtosis criterion to select the optimal analysis scales of MMF for processing fault signal. Shen *et al.* [23] adopted an adaptive scale MMF based on local peaks of raw signals. Li *et al.* [24] compared the noise suppressing performance of different types of MFs as well as envelopes, concluding that MMF has great potential of denoising signals. The other category is employing Mathematical morphological techniques to extract morphological features for realizing the identification of fault signals. The concepts of pattern spectrum [25] and morphology covering (MC) [26] are proposed originally by Maragos according to MM. Li *et al.* [27] and Zhao *et al.* [28] respectively employed morphological erosion operator and high-order differential morphological gradient to improve pattern spectrum. The MC technique has been adopted by Li *et al.* [29] to estimate morphological fractal dimension (MFD). Wang *et al.* [30] used the mathematical morphological fractal dimension to distinguish the performance degradation condition of the rolling bearing.

The focus of this paper is to research the denoising technology which can reduce the noise hidden in chaotic rolling bearing signals without destroying its original nonlinear dynamic structure. And then extract the chaotic feature for rolling bearing fault diagnosis. However, these denoising methods based on MMF are all based on the analysis of fault characteristic frequency, the denoising results of these methods mainly enhance the impact characteristics of fault signals. And in the progress of noise suppressing, the top-weakening distortion appears in the denoised waveform. The nonlinear dynamical structures of the system might be damaged.

In order to effectively distinguish faults of rolling bearing in the early stages. We propose a novel feature extraction method for rolling bearing early fault detection, which is based on chaos theory and mathematical morphology analysis. Firstly, the smooth multi-scale morphology filtering (SMMF) [31] method is employed to suppress the noise of the raw signal. SMMF solves the problem of topping distortion in morphological filtering. And the vibration signal of rolling bearing is able to be denoised and smoothed by SMMF without destroying its original nonlinear dynamic. Results

of SMMF denoising are compared with that of traditional denoising method to show its denoise ability for processing the simulation and experimental rolling bearing signals. And the denoised rolling bearing signals are reconstructed to obtain the phase plane. The existence of the strange attractor is testified that the vibration signal is chaotic. Besides, the composite multi-scale morphological fractal dimension (CMMFD) is proposed to quantify fractal characteristics of nonlinear rolling bearing signals under various conditions. Finally, the CMMFD feature is input into the classifier to achieve fault diagnosis. Hidden Markov model (HMM) [32] is an application of dynamic bayesian network, which has success in fault identification of rotating machinery. The HMM is a probabilistic statistical model with strong time series modeling ability, which can accurately represent the data characteristics in various states and is suitable for the recognition of time-varying nonstationary signals [33], [34]. HMM has a rich mathematical foundation, and features are able to be modeled by HMM as a random progress which can be estimated accurately by its related technology. Combined with feature engineering, HMM is easy to realize the learning and training of small data sets. In this paper, the chaotic features are trained and classified by HMM method to achieve an intelligent fault diagnosis system. The designed system is investigated on simulation and two data sets from rolling bearing test to evaluate the proposed technique.

To summarize, the novelties and contributions of this article mainly include four points:

1) To denoise rolling bearing signals without destroying its original nonlinear dynamic structure. The SMMF is first introduced to reduce the noise of bearing vibration data, which leverages the cubic B-spline interpolation algorithm to eliminate the top-weakening distortion of MMF denoised signal.

2) The CMMFD is first proposed measuring the self-similarity and irregularity of nonlinear signal, which can reflect the fractal characteristics and obtain more information about the signal by composite multi-scale analysis.

3) We propose a SMMF-CMMFD algorithm to extract chaotic features from vibration data set for rolling bearing fault diagnosis. And the CMMFD feature is input into the HMM classifier to achieve an intelligent fault diagnosis system.

The summary organization of the paper is as follows: The theory of SMMF is described in Section 2. Moreover, the corresponding optimization scheme of the algorithm is analyzed. Section 3 mentioned the concept of CMMFD. In Section 4, the scheme of the proposed method for fault diagnosis of rolling bearing is presented. The simulated, contaminated rolling bearing signals are analyzed in Section 5. Section 6 utilizes the proposed method and several comparison technologies to diagnose experimental data collected from the rolling bearing. Ultimate conclusions are presented in Section 7.

II. SMMF

A. MMF

Supposing that $f(n)$ is a one dimensional sequence, its domain is over the $F = (0, \ldots, N-1)$, and $g(m)$ is a unit SE with the domain $G = (0, \ldots, M-1)$, the defined value of M is supposed to be greater than the value of N. Four basic MF operations, the dilation, the erosion, the opening and closing, can be formulated as follows [35]:

$$(f \oplus g)(n) = \max\left[f(n-m) + g(m)\right], \; m \in 0, 1, \ldots, M-1 \tag{1}$$

$$(f \Theta g)(n) = \min\left[f(n-m) - g(m)\right], \; m \in 0, 1, \ldots, M-1 \tag{2}$$

$$(f \circ g)(n) = (f \Theta g \oplus g)(n) \tag{3}$$

$$(f \bullet g)(n) = (f \oplus g \Theta g)(n) \tag{4}$$

where $\oplus$ and Θ denote the dilation operation and the erosion operation, respectively. The dilation increases the valleys and enlarges the maxima of the processed object and the erosion reduces the peaks and enlarges the minima [36]. The symbol $\circ$ and symbol $\bullet$ indicate the closing operator and the opening operator, respectively. The opening operator flats the positive impulses and matches the negative impulses and the closing operator has the opposite effect [37]. In fact, it is difficult to obtain the prior information of a signal before processing. Therefore, according to four basic operations, a variety of combined morphological operators are proposed to process different actual signals. Such as the morphological gradient (MG) operator [38], is defined as:

$$MG(f(n)) = (f \oplus g)(n) - (f \Theta g)(n) \tag{5}$$

Filters of the open-closing operation (FOC) [39] and filters of close-opening operation (FCO) [40] are based on the ordinal opening and closing operation, are defined as following:

$$FOC(f(n)) = (f \circ g \bullet g)(n) \tag{6}$$

$$FCO(f(n)) = (f \bullet g \circ g)(n) \tag{7}$$

The combined morphological filter (CMF) is proposed to overcome problems of statistical bias of FOC and FCO. The CMF can flat signals by suppressing positive pulses and negative pulses of signals in the meantime. Which can be expressed as:

$$CMF(f(n)) = \frac{FOC(f(n)) + FCO(f(n))}{2} \tag{8}$$

MF in single-scale SE has limited efficiency in filtering the complex signals. The MMF is utilized to filter the target signal at different scales. Suppose λg is a SE at scale $\lambda(\lambda = 1, 2, \ldots k)$, the λg can be defined as:

$$\lambda g = \underbrace{g \oplus g \oplus \ldots \oplus g}_{\lambda - 1 \text{ times}} \tag{9}$$

The multi-scale MG, FOC, FCO, and CMF are separately expressed as:

$$MG(f(n)_{\lambda g}) = (f \oplus \lambda g)(n) - (f \ominus \lambda g)(n) \quad (10)$$

$$FOC(f(n)_{\lambda g}) = (f \circ \lambda g \bullet \lambda g)(n) \quad (11)$$

$$FCO(f(n)_{\lambda g}) = (f \bullet \lambda g \circ \lambda g)(n) \quad (12)$$

$$CMF(f(n)_{\lambda g}) = \frac{(f \circ \lambda g \bullet \lambda g)(n) + (f \bullet \lambda g \circ \lambda g)(n)}{2} \quad (13)$$

The morphological filter constructed by a SE at small scale can retain more detailed information of complex signals, but the effect of noise reduction is not obvious, while the morphological filter constructed by a SE at big scale has the obvious noise reduction ability, but it is possible to blur the details and cause waveform distortion. A single-scale MF filtering result represents a specific component hidden in the signal. Therefore, the morphological filtering at various scales is aggregated to obtain the multi-scale morphological analysis result of the noisy signal. The final output is expressed as:

$$Y = \sum_{j=1}^{j} \omega_j y_j \left(\sum_{j=1}^{j} \omega_j = 1 \right) \quad (14)$$

$$\omega_j = \frac{\sum_n R_j(n)^2}{\sum_j \sum_n R_j(n)^2}, \quad R_j(n) = f(n) - y_j(n) \quad (15)$$

where y_j is an output of MF at scale $j(j = 1, 2, \ldots, \lambda_{\max})$. ω_j denotes the weight coefficient of y_j. Y denotes the aggregate result. $R_j(n)$ is the residual amplitude difference (RAD) of MF.

B. THE CUBIC B-SPLINE INTERPOLATION

The output of the multi-scale morphological analysis is not smooth enough. That is to say, the local waveform of the signal denoised by MMF is undesirable rough. The top-weakening distortion appears in the large scale MF denoised waveform. However, it is finds that the distortion is regular all through. There is a distortion in local waveform, but the general shape of the entire waveform is retained. On the basis of the regularity of the distortion, the cubic B-spline interpolation algorithm is implemented to eliminate the influence of top-weakening distortion. The k-th B-spline function is expressed as following [41]:

$$P(t) = \sum_{i=0}^{n} d_i B_{i,k}(t), t \in [0, 1] \quad (16)$$

$$B_{i,0}(t) = \begin{cases} 1 & (t_i \leq t \leq t_{i+1}) \\ 0 & (\text{others}) \end{cases} \quad (17)$$

$$B_{i,k}(t) = \frac{t - t_i}{t_{i+k-1} - t_i} B_{i,k-1}(t) + \frac{t_{i+k} - t}{t_{i+k} - t_{i+1}} B_{i+1,k-1}(t) \quad (18)$$

where d_i $(i = 0, 1, \ldots, D)$ is the De Boor points, i is the serial-number of De Boor points, D is the total number. $t_0, t_1, \ldots, t_{D+k+1}$ are node vectors, $B_{i,k}(t)$ is a basic function,

Provide the 0/0 is zero. Let k be equal to 3, the B-spline function is the cubic polynomial over the domain [0,1], which is able to divide signals into some uniform segments. The processed signal has the advantage of detail smoothness. The cubic B-spline function is expressed as:

$$p(t) = \frac{(1-t)^3}{6} d_0 + \frac{3t^3 - 6t^2 + 4}{6} d_1 + \frac{-3t^3 + 3t^2 + 3t + 1}{6} d_2 + \frac{t^3}{6} d_3 \quad (19)$$

C. THE PROCESS OF SMMF

In order to solve the issue of the top-weakening distortion existing in traditional MMF and improve the precision of chaotic fault feature extraction, this section presents a method called SMMF to suppress the noise of contaminated chaotic vibration signals. The noise suppression process is shown in Fig. 1.
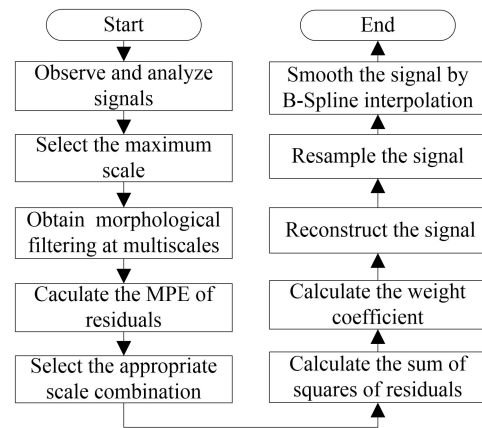

FIGURE 1. The flowchart of SMMF.

Work steps of SMMF are formulated as following:

Step 1: Observe and analyze the collected data.

Step 2: Select the shape of structural element. The flat SE is selected for denoising rolling bearing signal. It can retain characteristics of the waveform as much as possible [36]. The linear SE with a height of 0 is defined as the flat SE. Set the unit SE to {0, 0, 0}, which has the simplest algorithm and higher operational efficiency [20].

Step 3: Select the maximum scale of SE. The maximum-scale of SE is defined as $\lambda_{\max}$. Experiments demonstrate that the $\lambda_{\max}$ should be smaller than the sampling point in the fault period. Set f_s as the sampling frequency, and f_0 denotes the characteristic frequency. f_s/f_0 denotes the total number of sample points in a period. The characteristic frequency is defined as [42]:

$$f_0 = \sum_t \frac{2\pi N(t)}{t} \quad (20)$$

where $N(T)$ is defined as the number of turns performed in T. The maximal analytical scale of SE is determined to:

$$\lambda_{\max} = \lfloor f_s/f_0 \rfloor \quad (21)$$

where symbols $\lfloor \bullet \rfloor$ represents round down the number.

Step 4: Conduct CMF operation at different scales for morphological filtering, $\lambda_{\max}$ results are obtained.

Step 5: Choose the optimal structural element scale combination. Calculate the residual of each MF result. Then, calculate the multi-scale permutation entropy (MPE) [43] of residuals. The MPE is ultimately defined as following:

$$P^{(\tau)} = -\sum_{k=1}^{m!} p_k^{(\tau)} \ln p_k^{(\tau)} \qquad (22)$$

where $P^{(\tau)}$ is utilized to estimate the complexity and irregularity of the signal at the scale τ. k denotes the index of each element, m is the embedded dimension. The $\lambda_{best\tau}$ is defined as the optimal-scale of filtering rolling bearing signal at τ, which is the λ corresponding to the maximum value of $P^{(\tau)}$. The optimal combination is originally identified as $\Lambda = \{\lambda_{best1}, \lambda_{best2}, \ldots, \lambda_{best\tau}\}$. Remove recurring scales to ensure that each scale is used at most once.

Step 6: The weight coefficient of each scale is calculated.

Step 7: Reconstruct the signal.

Step 8: Smooth the signal. The MMF denoised signal is processed by the cubic B-spline interpolation technology.

III. MORPHOLOGICAL FEATURE EXTRACTION

A. MFD

The morphological covering technology proposed by Magaros and Schafer is used to calculate the fractal box dimension instead of Minkowski covering technology, the coverage area depends on the SE of morphological operators [26]. Compared with rule partition grid covering method, MC leads a more stable and preferable result [30]. The MFD is applied to measure self-similarity complexity of nonlinear signal. Its value is able to reflect the self-similarity and irregularity of chaotic signals. It is expressed as follows:

$$MFD = \lim_{\lambda \to 0} \frac{\log(A_{\lambda g}/\lambda^2)}{\log(1/\lambda)} \qquad (23)$$

where $A_{\lambda g}$ is the measurement of MC, namely morphological covers an area with SE on the scale λ. $f(n)$ is a one-dimensional discrete signal as mentioned in the previous section. The formula of $A_{\lambda g}$ is

$$A_{\lambda g} = \sum_{n=1}^{N} ((f \oplus \lambda g)(n) - (f \ominus \lambda g)(n)) = \sum_{n=1}^{N} MG_{\lambda g}(f(n)) \qquad (24)$$

The slop obtained by the least square linear fitting of $\log(A_{\lambda g}/\lambda^2)$ and $\log(1/\lambda)$ can be employed as the morphological fractal dimension of $f(n)$ [29].

B. CMMFD

On most occasions, different types of faults lead to various changes in terms of morphological fractal dimension. Therefore, the MFD as a feature can be applied to classify different fault signals. However, different from the strict fractal structure, fault signals are not strictly self-similar, the assumption of a constant fractal dimension at all scales may not be strictly accurate [44]. A single-scale MFD is

not enough to represent all information of nonlinear signal [45]. The division of fault state space may overlap if the fractal dimension values of two fault signals are close. The multi-scale analysis can reflect the complexity characteristics and obtain more information about the signal. The CMMFD is proposed to measure the self-similarity and irregularity or complexity of nonlinear signal.

Supposing that the scale ε is defined as the window length of coarse-grained process. Firstly, the $f(n)$ is coarsely granulated with a scale ε. The process of the composite coarse granulation of time series is expressed as:

$$\{z_{h,l}^{(\varepsilon)}\} = \frac{1}{\tau} \sum_{n=(l-1)\varepsilon+h}^{l\varepsilon+h-1} f(n) \qquad (25)$$

where $l = 1, 2, \ldots, \lfloor N/\varepsilon \rfloor$, $h = 1, 2, \ldots, \varepsilon$, $\lfloor \bullet \rfloor$ denotes downward rounding. The composite multi-scale technology is adopted by CMMFD to coarse grain the sequence $f(n)$. Then, the MFD of each composite coarse-grained sequence under this scale is calculated. Finally, the CMMFD under scale factor ε is obtained by averaging. We define the composite multi-scale morphological fractal dimension as:

$$CMMFD(f, \lambda, g, \varepsilon) = \frac{1}{\varepsilon} \sum_{h=1}^{\varepsilon} MFD(z_h^{(\varepsilon)}, g, \lambda) \qquad (26)$$

IV. THE PROPOSED FAULT DIANOSIS SCHEME

In order to achieve fault classification of chaotic rolling bearing data. The SMMF is employed to denoise the chaotic signal. And the CMMFD feature is extracted to quantify the rolling bearing signals. Then the features are input into HMM for fault diagnosis. The whole diagnostic scheme is shown in Fig. 2.

As shown in Fig. 2, the process is formed from four parts:

(1) Vibration signal collection. Rolling bearing vibration data is collected through the signal acquisition device. Then, reconstruct the phase plane for rolling bearing vibration signals, observe the attractors of figures under different conditions.

(2) Noise reduction. The SMMF denoise the signal without improving the problem of topping distortion in morphological filtering. And it is superior to other methods for the noise suppression performance of contaminated chaotic signals. In order to retain the nonlinear dynamical structures of the original signal. The noise of collected fault rolling bearing signal is adaptively suppressed by the denoising method SMMF.

(3) Chaotic feature extraction. The CMMFD feature can reflect the fractal characteristics and obtain more information about the signal by composite multi-scale analysis. Thus, we extract CMMFD as a chaotic feature to measure the self-similarity and irregularity of nonlinear signal. Firstly, the denoised rolling bearing was coarsely granulated at the scale of ε by a composite multi-scale coarse-grain technology, and ε coarse-grain sequences are obtained. Then, calculate the $A_{\lambda g}$ of each coarse-grained sequence under this
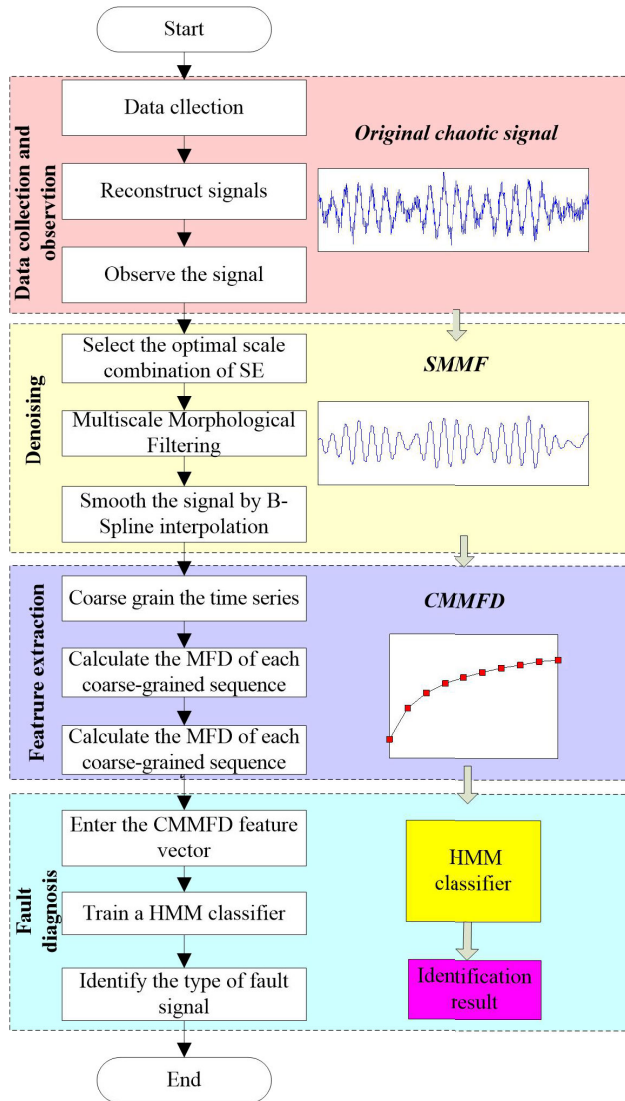
FIGURE 2. The flowchart of fault diagnosis scheme.

scale ε, and the slope obtained by the least square linear fitting of $\log(A_{\lambda g}/\lambda^2)$ and $\log(1/\lambda)$ can be employed as the estimation of MFD of each coarse-grain sequence. Finally, the CMMFD under scale factor ε is obtained by averaging the MFDs at scale factor $1, 2, \ldots, \varepsilon$.

(4) Fault diagnosis. HMM is easy to combine with feature engineering and it has success in fault identification of rotating machinery. We select HMM algorithm to realize the learning and training of rolling bearing data sets. The CMMFD feature extracted from a part of different rolling bearing data sets used as the input vector to train a HMM fault classifier. Then, all rolling bearing data sets are tested by the classifier.

V. NUMERICAL VALIDATION

A. NUMERICAL SIMULATION MODEL WITH BEARING LOCALIZED DEFECT

The simulation of rolling bearing was taken to verify the effectiveness of the proposed scheme. Consider the dynamic

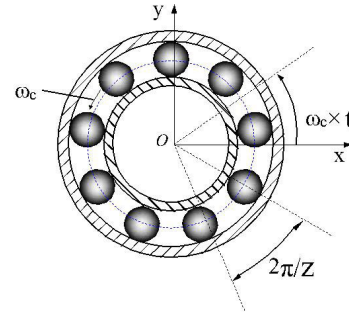model of a rolling bearing developed by Rafsanjani [46], which is shown in Fig. 3.

FIGURE 3. The model of rolling bearing.

This bearing vibration numerical model with a local damage is simulated by a nonlinear two-degree of freedom vibration system. The differential equations are as follows:

$$
\begin{aligned}
m\ddot{x} + c\dot{x} + f_x &= W_x + f_u \cos \omega t \\
m\ddot{y} + c\dot{y} + f_y &= W_y + f_u \sin \omega t
\end{aligned}
\tag{27}
$$

where m denotes the equivalent mass of the inner race along with the rotor to prop up by rolling bearing. c represents equivalent damping. W_x and W_y indicate the radial load component in the x and y directions of rotor, f_u represents unbalance force. f_x and f_y are the restoring force, and the formulas are:

$$
f_x = K \sum_{q=1}^{Z} \gamma_q \delta_q^{1.5} \cos \theta_q
$$

$$
f_y = K \sum_{q=1}^{Z} \gamma_q \delta_q^{1.5} \sin \theta_q
\tag{28}
$$

where Z denotes the number of rolling elements, and K is defined as the contact stiffness, which can be calculated based on Hertzian deformation local to the contact zone [46]. δ_q represents the overall contact deformation of the q-th rolling element, γ_q is defined as the loading area variable, θ_q indicates the angular position, which can be calculated according to the cage frequency ω_c and the initial position of rolling element.

The Runge-Kutta-Felhberg method which corresponds to the function ode45 in MATLAB was utilized to solve dynamic equations. The 6205 deep groove ball bearing was applied in the simulation. The sampling frequency is set to 48kHz. The shaft rotational speed is 1800 rpm. The maximum defect depth is 0.1 mm, the defect diameter is 1 mm. Dimensions of the bearing were presented in Table 1.

TABLE 1. The dimensions of the ball bearing.

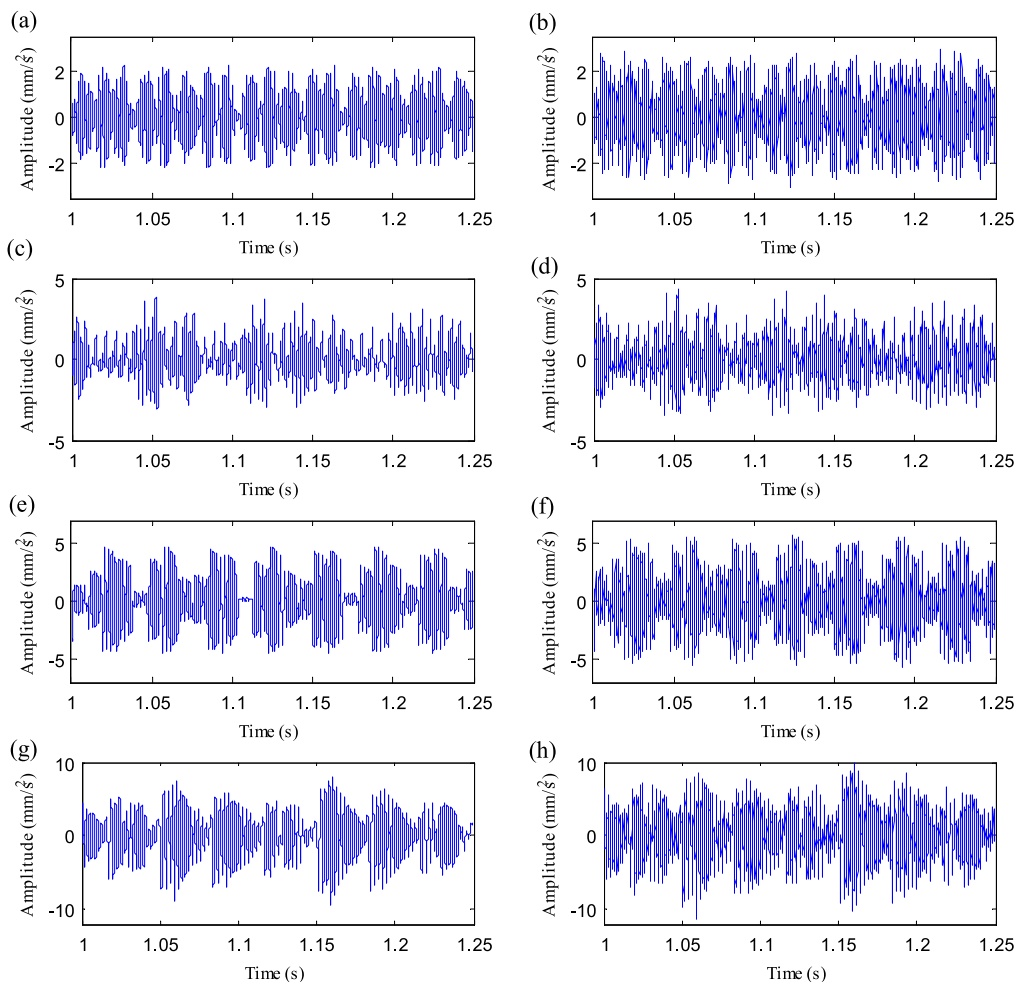| Roller diameter	Pitch diameter	Number of rolling elements	Contact angle
8.0 mm	38.5 mm	9	0°

FIGURE 4. The vertical accelerations of simulated bearing system: (a) original normal bearing signal, (b) noisy normal bearing signal, (c) original inner race fault signal, (d) noisy inner race fault signal, (e) original outer race fault signal, (f) noisy outer race fault signal, (g) original ball fault signal, (h) noisy ball fault signal.

The acceleration response of simulated bearing system usually takes a period of time to achieve a stable state. So the simulated experimental data are collected from 1 s. The simulated signal was superimposed with Gauss white noise to simulate the real rolling bearing fault signal as far as possible. The Gaussian white noise denotes the running noise interference of the device. The contaminated bearing signal consists of corresponding clean signal and Gaussian white noise. The *SNR* is expressed as following:

$$SNR = 10 \log_{10} \frac{\sum_t \hat{x}^2(t)}{\sum_t \left(x(t) - \hat{x}(t)\right)^2} \quad (29)$$

where $\hat{x}(t)$ and $x(t)$ indicates the clean signal and contaminated time series in the progress of calculating the input signal to noise ratio (SNR_{in}). For the output signal to noise ratio (SNR_{out}), $\hat{x}(t)$ indicates the and denoised signal and $x(t)$ is contaminated signal.

The simulated original and the contaminated horizontal acceleration response of normal bearing are illustrated in Fig. 4 (a) and (b). The original signal of the bearing system with a localized defect on the inner raceway is illustrated in Fig. 4 (c), and the contaminated signal is shown in Fig. 4 (d). The original and contaminated outer race fault signals are shown in Fig. 4 (e) and (f). The horizontal acceleration responses with a localized defect on the rolling elements are shown in Fig. 4 (g) and (h).

Different faults cause various influences on non-linear dynamics of the rolling bearing system. These phase planes can be used to represent the obvious nonlinear change of system dynamic. Fig. 5 (a) -(h) illustrate the reconstructed phase plane of the simulated original and contaminated rolling bearing vibration signals. The attractors are observed from phase plane of different conditions. For clean signals, the trajectories of attractors are self-similar and regular, and the shape of strange attractors for different conditions is different. The normal rolling bearing and defective rolling bearing can be distinguished by comparing the attractors of different
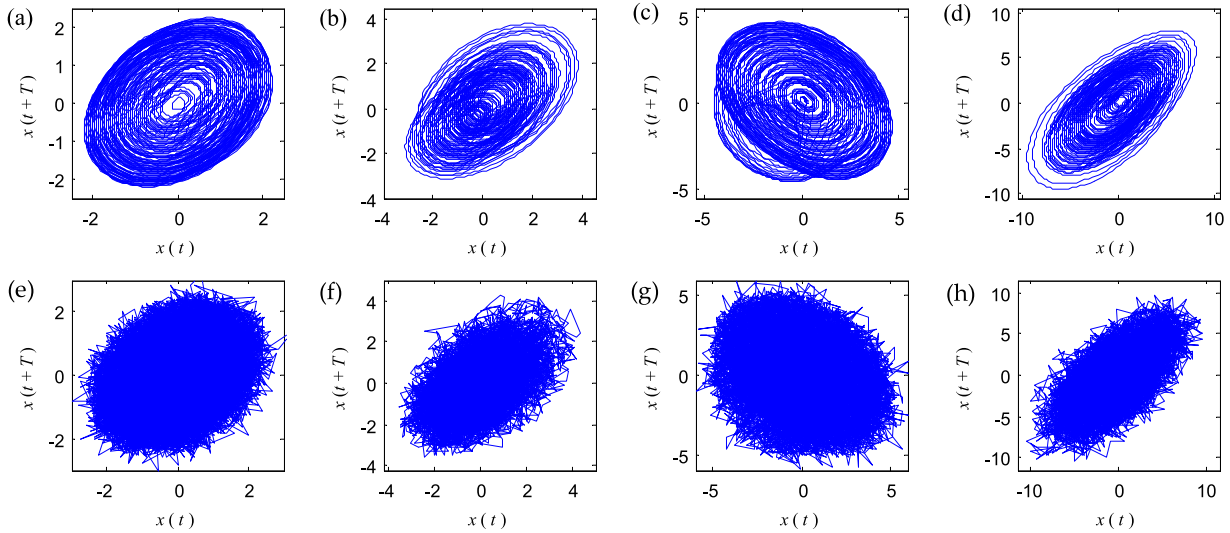
FIGURE 5. The phase plane for simulated rolling bearing vibration signals: (a) original normal bearing signal, (b) original inner race fault signal, (c) original outer race fault signal, (d) original ball fault signal, (e) noisy normal bearing signal, (f) noisy inner race fault signal, (g) Noisy outer race fault signal, (h) noisy ball fault signal.

clean signals. But for contaminated signals, the trajectories of attractors are disordered and irregular. It is hard to classify different fault signals.

B. NOISE SUPPRESION

These simulated signals above are analyzed by the mentioned SMMF algorithm to verify its effectiveness for contaminated nonlinear rolling bearing vibration signals. For a comparison, three common noise suppression methods are used to process the same simulated rolling bearing vibration signals. The first denoised method is the clear first iterative thresholding based on EMD (EMD-CIIT) [47], and the iteration is set at 15. The second method is wavelet threshold (WT) [13]. The soft threshold is used to process signals, and the noise reduction was done under the following conditions: db8, level 4 decomposition. The traditional MMF without smoothing is also compared with SMMF, as one of the common noise suppression methods.

Fig. 6 illustrates the projection of phase trajectories for the signal denoised by the mentioned algorithms. Fig. 6 (a1) -(a4) show the denoising results by EMD-CIIT for four contaminated rolling bearing signals. Fig. 6 (b1) -(b4) show the denoising results by WT algorithm. As seen in these figures, the shape of the reconstructed phases are almost approximately the same as the original signals, but the phase trajectories of denoised signals are obviously rougher than that of the original signal. Fig. 6 (c1) -(c4) show the filtering results of MMF, the phase trajectories of the restored attractor are obviously deformed, which makes the original ordered self-similar structures appear disorderly. The denoise results for 4 simulated contaminated rolling bearing signals by SMMF algorithm are illustrated in Fig. 6 (d1)-(d4). Attractors of four types rolling bearing signals processed by

SMMF are similar to those reconstructed by the original signals, and the orbits are more regular than the orbits obtained by other denoising technologies.

The SNR_{out}, the root mean square error (RMSE) [14], and the MFD indexes are applied to assess the effect of noise suppression for the sake of verifying the effectiveness of denoising algorithms intuitively. The RMSE is expressed as:

$$RMSE = \sqrt{\frac{1}{N} \sum_t (x(t) - \hat{x}(t))^2} \qquad (30)$$

Table 2 and Table 3 show the SNR and RMSE of different rolling bearing signals before and after noise reduction by 4 algorithms. The SNR_{in} of contaminated signals is 10 dB. From the tables, it can be seen that the output SNR of all denoising methods are increased compared with the input SNR, and the $RMSE$ of signals are decreased after denoising by three algorithms. In addition, the proposed SMMF is the highest SNR and $RMSE$ improvement, especially in terms of SNR, increased at least 13 dB. This proves that the SMMF can effectively remove the noise hidden in the chaotic simulated signal.

TABLE 2. The SNR_{out} comparison among different algorithms.

Algorithms	Normal bearing	Inner race fault	Outer race fault	Ball bearing fault
EMD-CIIT	17.4305	19.5185	20.2283	19.8155
WT	18.7322	17.9833	19.0486	16.0846
MMF	17.4733	18.6007	18.5652	17.5664
SMMF	24.2632	24.2093	24.9270	24.1135

The MFD can reflect the self-similarity and irregularity of chaotic signals. Set the analytical scale as $\lambda = [2^1, 2^2, \ldots, 2^8]$. Table 4 shows the MFD of different rolling
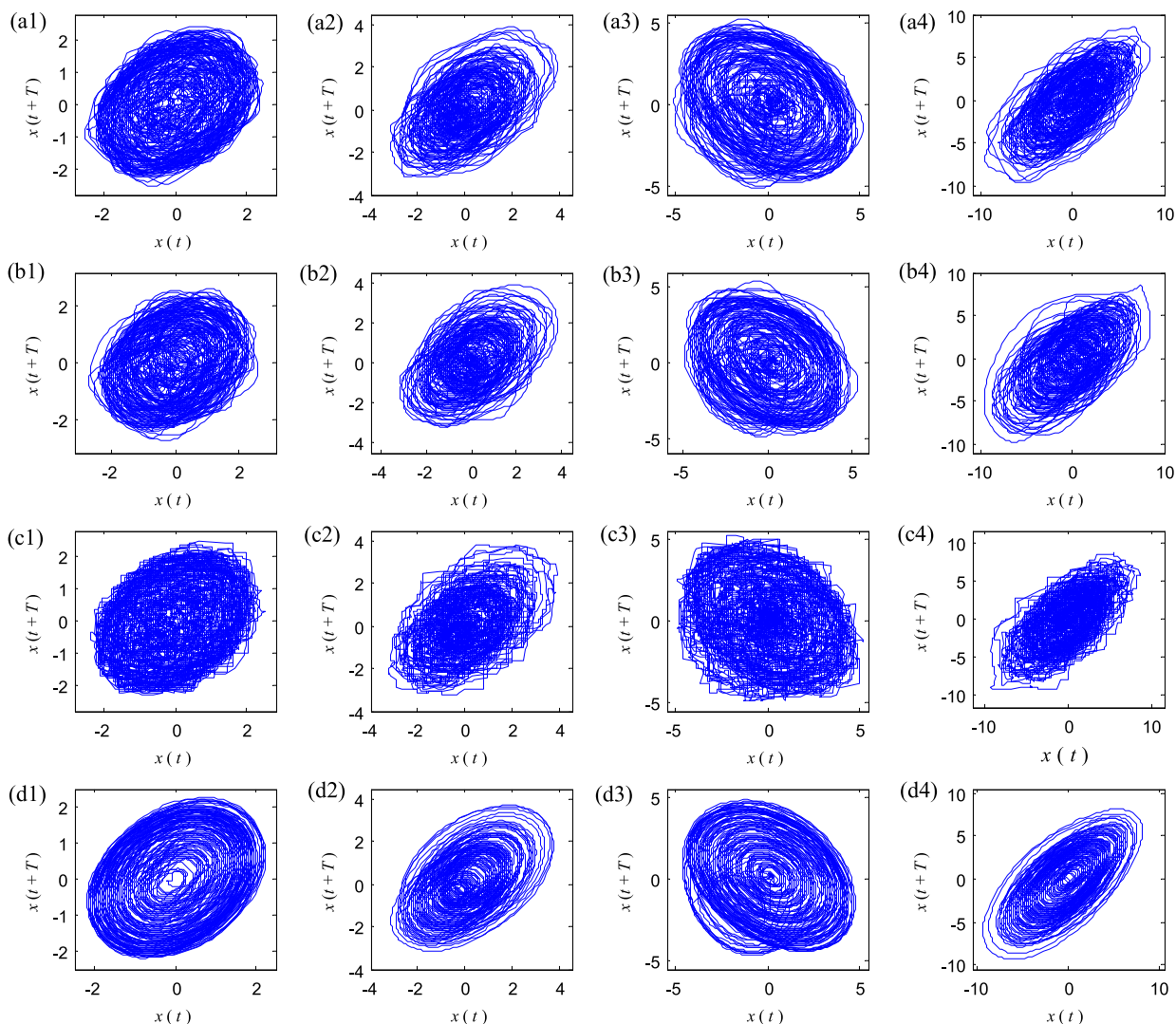
FIGURE 6. The reconstructed phase plane for denoised rolling bearing signals: (a1) -(a4) are signals denoised by EMD-CIIT, (a1) normal bearing, (a2) inner race fault, (a3) outer race fault, (a4) ball fault, (b1) -(b4) are signals denoised by WT, (b1) normal bearing, (b2) inner race fault, (b3) outer race fault, (b4) ball fault, (c1) -(c4) are signals denoised by MMF, (c1) normal bearing, (c2) inner race fault, (c3) outer race fault, (c4) ball fault, (d1) -(d4) are signals denoised by SMMF, (d1) normal bearing, (d2) inner race fault, (d3) outer race fault, (d4) ball fault.

TABLE 3. The *RMSE* comparison among different algorithms.

Algorithms	Normal bearing	Inner race fault	Outer race fault	Ball bearing fault
EMD-CIIT	0.0966	0.1300	0.2129	0.4449
WT	0.1219	0.1673	0.2648	0.4845
MMF	0.1454	0.1479	0.2749	0.4582
SMMF	0.0665	0.0725	0.1223	0.2137

bearing signals before and after noise reduction by 4 algorithms. The noise of signals leads to increase in space-filling means that noise results in an increase in the MFD. As shown in Table 4, the MFD for non denoised signal is higher than denoised signal. The MFD of the signal rolling bearing for different conditions after denoising by above methods was decreased. The MFD of the signal which is denoised by

SMMF is the closest to the original signal. It means the fractal dimensions measuring and self-similarity or irregularity of signal denoised by SMMF is the most similar to the original signal.

As seen in Table 4, the MFD of faulty rolling bearing signals are lower than the MFD of healthy bearing signals. It indicates that the projection of the normal bearing contains a higher density attractor. Different types of faults have various shapes and density of attractors. Therefore, morphological fractal dimensions of diverse faults are different. However, the noise of signals leads to increases of space-filling, then, the density of attractors increases. Which leads to an increase in the MFD. The MFD of contaminated healthy/faulty signal is close to each other, which indicates that the MFD of signal is susceptible to noise. Thus, the morphological fractal dimension should be extracted after noise reduction.
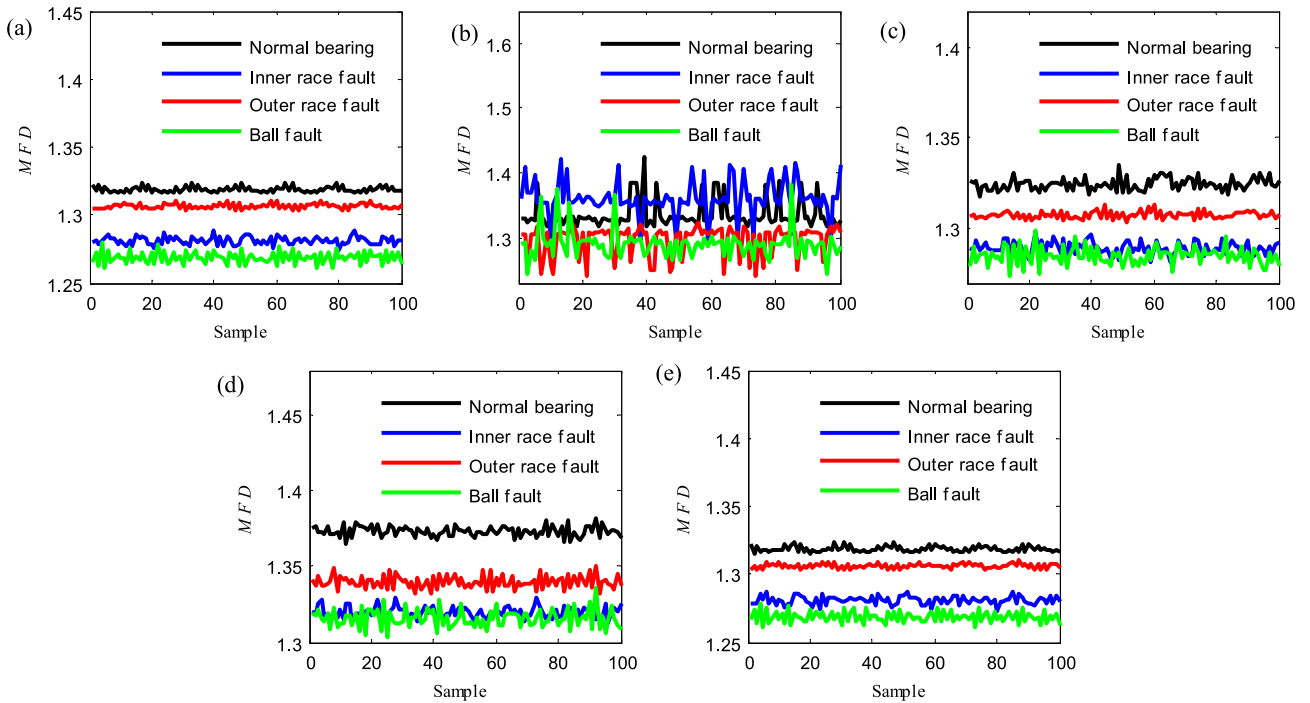
FIGURE 7. The MFD of original signals and denoised bearing signals: (a) original bearing signals, (b) EMD-CIIT denoised signals, (c) WT denoised signals, (d) MMF denoised signals, (e) SMMF denoised signals.

TABLE 4. The MFD comparison among different algorithms.

Algorithms	Normal bearing	Inner race fault	Outer race fault	Ball bearing fault
Contaminated signal	1.5293	1.5113	1.5151	1.5367
Original signal	1.3172	1.2808	1.3003	1.2650
EMD-CIIT	1.3836	1.3040	1.3071	1.2878
WT	1.3325	1.3003	1.3060	1.2833
MMF	1.3403	1.3114	1.3275	1.3143
SMMF	1.3169	1.2790	1.3004	1.2660

C. FEATURE EXTRACTION

After the noise reduction process, the existence of attractors was observed for healthy/faulty signals. These orbits in the phase plane indicate the dynamics characteristic of non-linear vibration. The morphological fractal dimension was exacted to quantify complexity of those orbits. The sampling length of each simulated normal/fault rolling bearing was 409600. Each signal is divided into 100 samples. Thus a total of 400 samples were collected in the simulated experiment. The MFD for each group simulated signal was calculated. Fig. 7 demonstrates the MFD for different types rolling bearing signals and which were denoised by the mentioned 4 technologies. For fractal signal, the fractal dimension should be close to a constant, even if the faulty bearing signal isn't an expected self-similarity. Clearly, these signals denoised by SMMF algorithm achieve the best result for calculated the MFD of 100 samples. The MFD of signals denoised by WT also gives some promising values. However, the variation

from the MFD is much more significant than that of SMMF denoised signals, and the state space of the inner fault signals and ball fault signal coincides seriously. The signals denoised by EMD-CIIT and MMF failed to obtain reasonable MFD. The range of features that are exacted from each type of signal processed by EMD-CIIT has an evident fluctuation. The state space of different faults is not clearly divided. The MFD exacted from normal rolling bearing signal processed by MMF method is far away from the MMF of the original signal. The division of fault state space may overlap if the fractal dimension values of two fault signals are close.

In order to comprehensively measure the complexity of the signal. The CMMFD was applied to characterize the chaotic feature of simulated rolling bearing signals for four conditions. Fig. 8 illustrates the CMMFD for different types clean /denoised rolling bearing signals. As seen in the figures, the fractal dimension at different scale factors of the same signal is not the same with each other. Even if the MFD at some scale factor of different type signals overlapped with the other conditions, it can be discriminated from different scales.

D. DIAGNOSIS RESULTS

According to the mentioned feature extraction scheme. The MFD and CMMFD extracted from signals denoised by different methods were used to form features space. To evaluate the performance of four denoised technology and two nonlinear features. These fractal features were used as input of training HMM for fault identification. A classifier consists of four
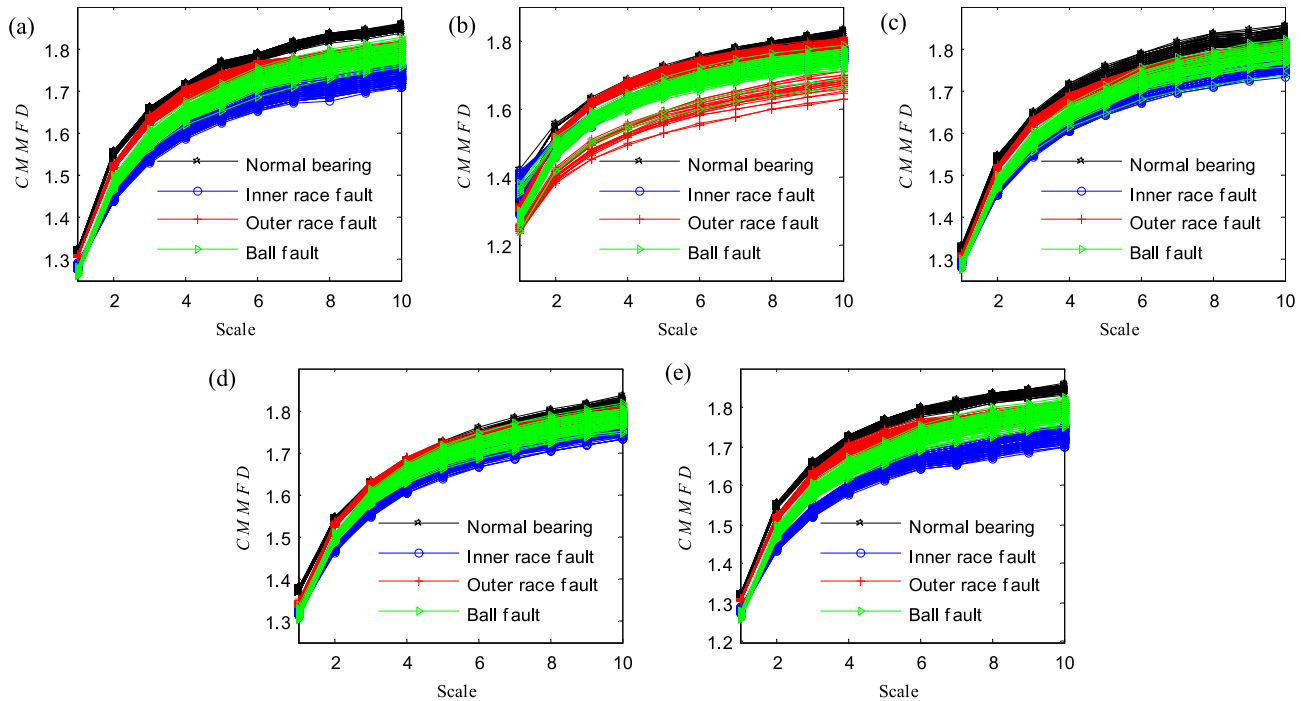
FIGURE 8. The CMMFD of original signals and denoised bearing signals: (a) original bearing signals, (b) EMD-CIIT denoised signals, (c) WT denoised signals, (d) MMF denoised signals, (e) SMMF denoised signals.

TABLE 5. Fault identification results.

Algorithms	Normal bearing (%)	Inner race fault (%)	Outer race fault (%)	Ball bearing fault (%)
EMD -MFD	89	77	73	67
WT -MFD	100	72	85	69
MMF-MFD	100	50	88	77
SMMF -MFD	100	98	100	89
EMD -CMMFD	98	85	91	92
WT -CMMFD	100	91	95	88
MMF-CMMFD	100	99	90	98
SMMF -CMMFD	100	100	100	100

HMM models, which are trained by the first 40 samples of each type of faulty/normal signal. Then 100 samples were input into classifiers for testing. Finally, the HMM classifier specifies output the fault type as the output. Fault identification results of simulated rolling bearing data are presented in Table 5.

As seen in Table 5, most samples are identified as the correct type by using MFD features. The identification results of the MFD feature extracted from EMD denoised signals are the worst performance among four denoisng methods. MFD features extracted from WT denoised signals are good for a normal data set. However, other types of fault signal performance a poor classification. Also, results of MFD features extracted from MMF signals are good for normal data sets, but the identifying result of the other faults are not desirable.

Although the success rate of rolling ball identification is 90%. MFD features extracted from SMMF denoised data sets show the best results among the four denoising algorithm.

Using the CMMFD features, the classification performance of CMMFD features extracted from the noise reduced signal by the same denoising technology are much better than that of MFD features. The CMMFD features extracted from EMD denoised signals can identify normal condition with a 98% rate, and the success rate of other faults has been greatly improved also. Classification results of CMMFD features extracted from WT denoised inner race and rolling ball fault signals increased by 19% correct rate, and outer race fault by 10%. The identification performance obtained by CMMFD features which extracted from MMF denoised signals are good for most data sets except outer race fault. The SMMF-CMMFD scheme shows best results among all schemes for identifying different types of fault. This scheme can classify different simulated rolling bearing faults with a 100% rate. These identification results demonstrate that the proposed scheme can classify different simulated rolling bearing faults exactly.

VI. EXPERIMENTAL VERIFICATION
In this section, two experimental rolling bearing data sets were analyzed to verify the performance of the mentioned approach. Also, the analysis results were compared with some contrastive schemes to prove its advantages of feature extraction.
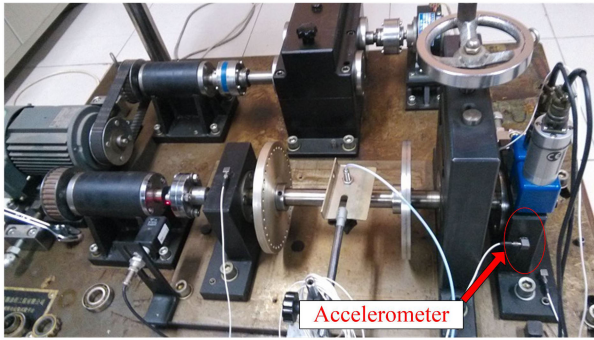
FIGURE 9. The rolling bearing fault experimental bench.

A. CASE 1: ROLLING BEARING DATA WITH FUZZY ORBITS OF ATTRACTORS

The QPZZ test device is illustrated in Fig. 9. The motor is fixed on the test-bed, which is the power source of the bearing simulation device, its speed was 1470 rpm in the experiment. In the experiment, the LYC6205E deep groove ball bearing was utilized as experimental bearing, which was mounted on the far right end of the rotation shaft. Table 6 shows geometrical parameters of experimental rolling bearing. The vibration experiment data are collected by accelerometer fixed on

TABLE 6. Parameters of experimental bearing.

Roller diameter	Pitch diameter	Number of balls	Contact angle
7.94 mm	38.5mm	9	0°

bearing housing of the bench. The sampling frequency of the vibration signal was 12800 Hz. The data collection for four types of healthy/faulty conditions of rolling bearing: normal bearing, localized defect on the inner race, localized defect on the outer race, localized defect on rolling element. The fault size is 0.2 mm in width and 1.5 mm in depth. Fig. 10 shows the first 6400 points data collected in four conditions.

Fig. 11 shows the reconstructed phase plane of the original vibration signals. It can be observed from Fig. 11 that the trajectories of the original signals are disordered and irregular. It is difficult to distinguish between different fault signals. Also, it is difficult to quantify the complexity of those orbits by fractal dimension. Disordered orbits of attractor represent that the signal is polluted by noise while the attractor with smooth orbits is less polluted by noise, but these are not strictly correlated. In general, denoising technology is capable of suppressing the noise mixed with the ball bearing
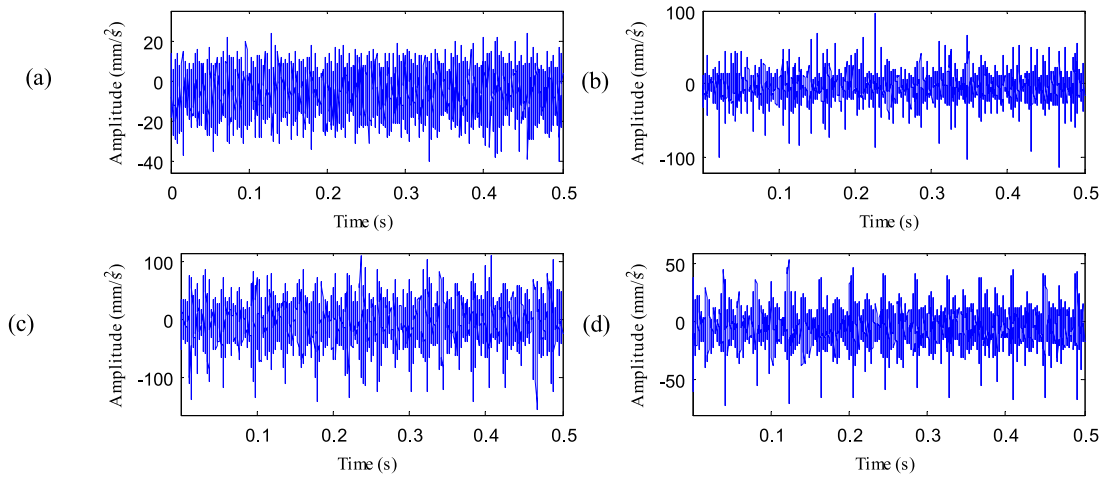

FIGURE 10. The experimental rolling bearing vibration signals: (a) normal bearing, (b) inner race fault, (c) outer race fault, (d) ball fault.
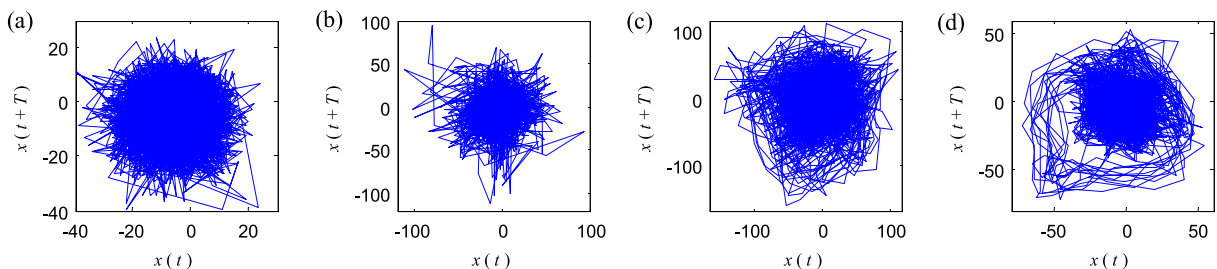

FIGURE 11. The reconstructed phase plane for rolling bearing vibration signals: (a) normal bearing, (b) inner race fault, (c) outer race fault, (d) ball fault.
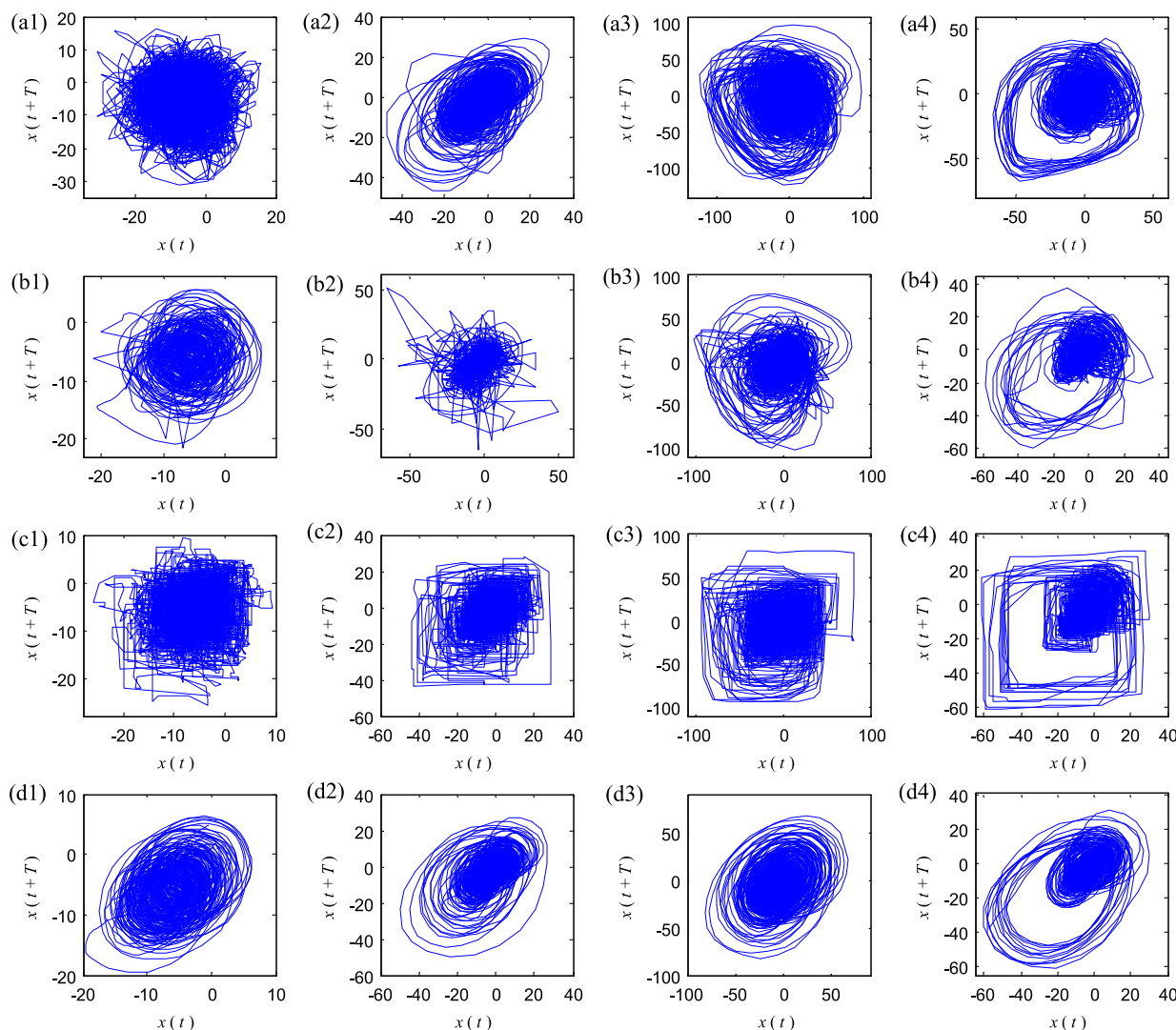
FIGURE 12. The reconstructed phase plane for denoised rolling bearing signals: (a1) -(a4) are signals denoised by EMD-CIIT, (a1) normal bearing, (a2) inner race fault, (a3) outer race fault, (a4) ball fault, (b1) -(b4) are signals denoised by WT, (b1) normal bearing, (b2) inner race fault, (b3) outer race fault, (b4) ball fault, (c1) -(c4) are signals denoised by MMF, (c1) normal bearing, (c2) inner race fault, (c3) outer race fault, (c4) ball fault, (d1) -(d4) are signals denoised by SMMF, (d1) normal bearing, (d2) inner race fault, (d3) outer race fault, (d4) ball fault.

signal and obtaining a time series governed by deterministic dynamics. Therefore, four denoisng technologies are applied to progress the original experimental signal.

Fig. 12 shows the projection of phase trajectories of the signal denoised by four mentioned algorithms. The processed results by EMD-CIIT are illustrated in Fig. 12 (a1) -(a4). As seen in the figures, the attractors can be observed clearly from the inner race fault signal, outer race fault signal, and ball bearing fault signal. But for the reconstructed normal signal, trajectories of reconstructed normal rolling bearing signal are disorderly as before denoising. The shape of attractor can not be observed at all. Fig. 12 (b1) -(b4) shows denoising results of WT method. The trajectories of the reconstructed normal signal are smoother than EMD-CIIT processing signal. But the denoised results of the other signals are not expected. Fig. 12 (c1) -(c4) illustrate the projection

of phase trajectories of the signal denoised by MMF. The shapes of attractors reconstructed by the four types of signals are clear, but the trajectories of attractors are not smooth. The phase diagrams for the reconstructed SMMF denoising signals are illustrated in Fig. 12 (d1) -(d4). It is clear to see that the attractor of the signal denoised by SMMF can be observed easily. And trajectories of attractors are smooth and the shape is clear. By comparing the denoising results of different methods, it can be inferred that the SMMF has better denoising effect on noisy rolling bearing signals than the other three methods.

MFD and CMMFD features are extracted from the signal denoised by four mentioned methods, respectively. Fig. 13 illustrates the MFD extracted from rolling bearing samples. The MFD that exacted from each type of the signal processed by EMD-CIIT has an evident fluctuation as
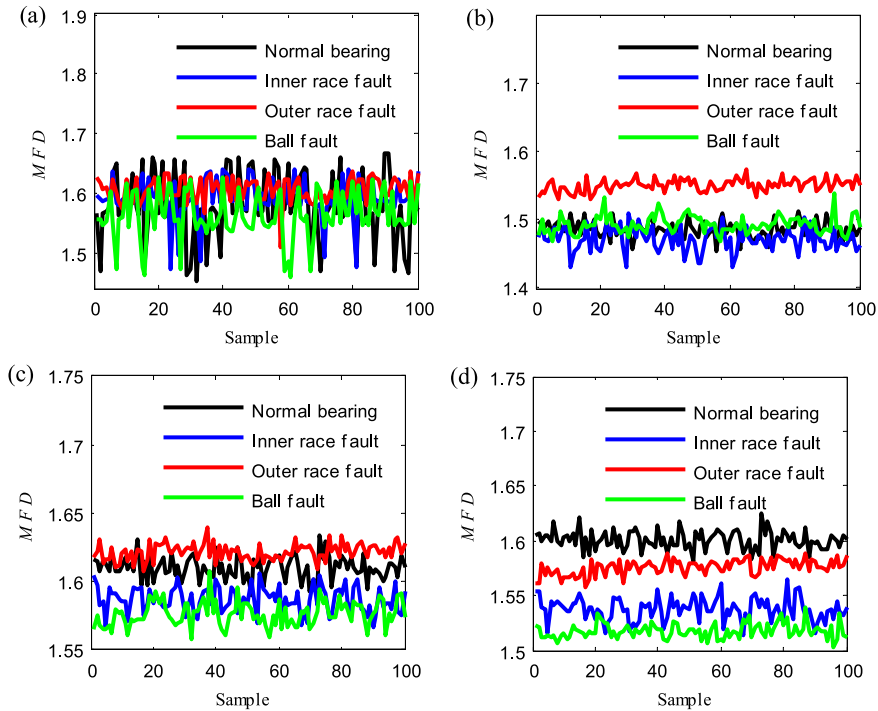
FIGURE 13. The MFD of denoised bearing signals: (a) EMD-CIIT denoised signals, (b) WT denoised signals, (c) MMF denoised signals, (d) SMMF denoised signals.
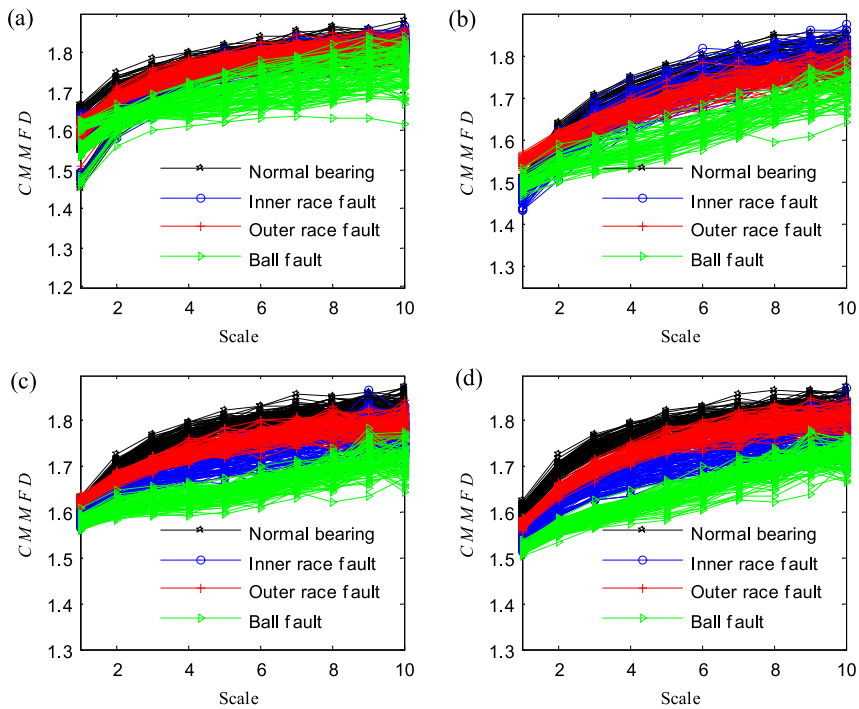

FIGURE 14. The CMMFD of denoised bearing signals: (a) EMD-CIIT denoised signals, (b) WT denoised signals, (c) MMF denoised signals, (d) SMMF denoised signals.

it can be observed in Fig. 13 (a). We can find a striking overlap among the state space of different faults. Fig. 13 (b) shows the MFD that exacted from the signal processed by

WT, the fluctuation of the results is smaller than that of EMD-CIIT. But the state space division of 3 types of fault bearing signals is still intersecting. Fig. 13 (c) shows the
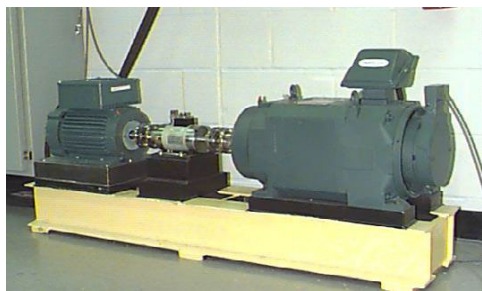
FIGURE 15. The rolling bearing fault experimental bench.

MFD exacted from signals processed by MMF method. The state space of MMFs extracted from fault signal and normal signal are overlap. It is worth noting that the value of MFDs extracted from normal signals denoised by WT or MMF are smaller than the value of outer race fault signal, which is not reasonable. Fig. 13 (d) illustrates the MFD exacted from signals processed by SMMF. The state space of inner race signal and the state space of ball fault signals are slightly crossed. CMMFD features extracted from denoised signal are expressed in Fig. 14. It can be observed that, for $\tau = 1$, all the four methods give a overlap state space of 4 four bearing states, which is the same as the MFD. For $\tau \geq 2$, the CMMFD obtained from the EMD-CIIT denoising signal still present worse discriminative capacity to four bearing signals, as shown in Fig. 14 (a). The CMMFD features extracted from the WT technique denoising signal are displayed in Fig. 14 (b). CMMFD features of outer race fault signals and ball fault signals can be differentiated from other types. But for normal bearing and inner race fault signals, it gives almost all overlap CMMFD features. The CMMFD which is extracted from MMF and SMMF denoising signals are depicted in Fig. 14 (c) and (d). The state space composed of CMMFD feature vectors extracted from the MMF and

SMMF denoised signals are superior than that of EMD-CIIT and WT denoised signals.

The MFD and CMMFD extracted by 4 methods are employed as feature vectors for distinguishing bearing states, they are applied as input to train the HMM classifier, then the feature set is distinguished. Table 7 lists the fault classification results of each feature vector as the input of HMM. Comparing the features extracted from the same rolling bearing signals, the proposed SMMF-CMMFD technique achieves better distinguish results. For the other compared techniques, most samples are given the right classify results, but they cannot distinguish all of rolling bearing data, and some samples are given false results.

TABLE 7. Fault identification results.

Algorithms	Normal bearing (%)	Inner race fault (%)	Outer race fault (%)	Ball bearing fault (%)
EMD -MFD	89	77	73	67
WT -MFD	100	72	85	69
MMF-MFD	100	50	88	77
SMMF -MFD	100	98	100	89
EMD -CMMFD	98	85	91	92
WT -CMMFD	100	91	95	88
MMF-CMMFD	100	99	90	98
SMMF -CMMFD	100	100	100	100

B. CASE 2: BEARING DATA WITH CLEAR ORBITS OF ATTRACTOR

The second data set is collected from the ball bearing test device of Case Western Reserve University bearing data center [48]. As shown in Fig. 15, the electric motor, the transducer/encoder and the dynamometer are fixed on the test bench. The fault/normal test rolling bearing are used to support the shaft of an electric motor. And an accelerometer is mounted to collect acceleration data. A deep groove rolling bearing SKF 6205 with 0.007 in. (0.178 mm) diameters and
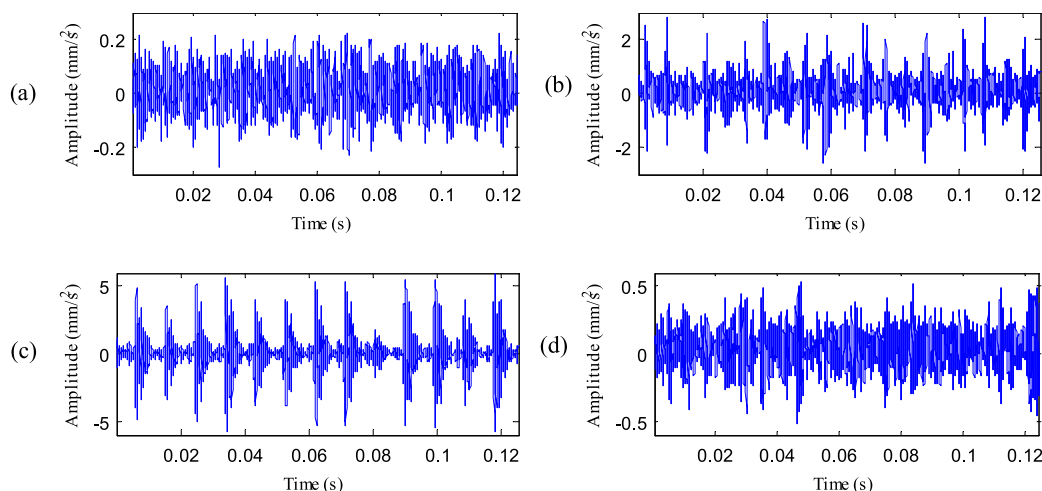

FIGURE 16. The experimental rolling bearing vibration signals: (a) normal bearing, (b) inner race fault, (c) outer race fault, (d) ball fault.
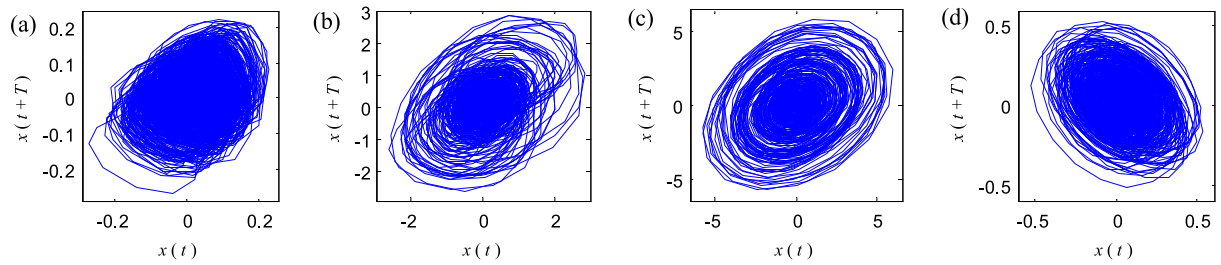
FIGURE 17. The reconstructed phase plane for rolling bearing vibration signals: (a) normal bearing, (b) inner race fault, (c) outer race fault, (d) ball fault.
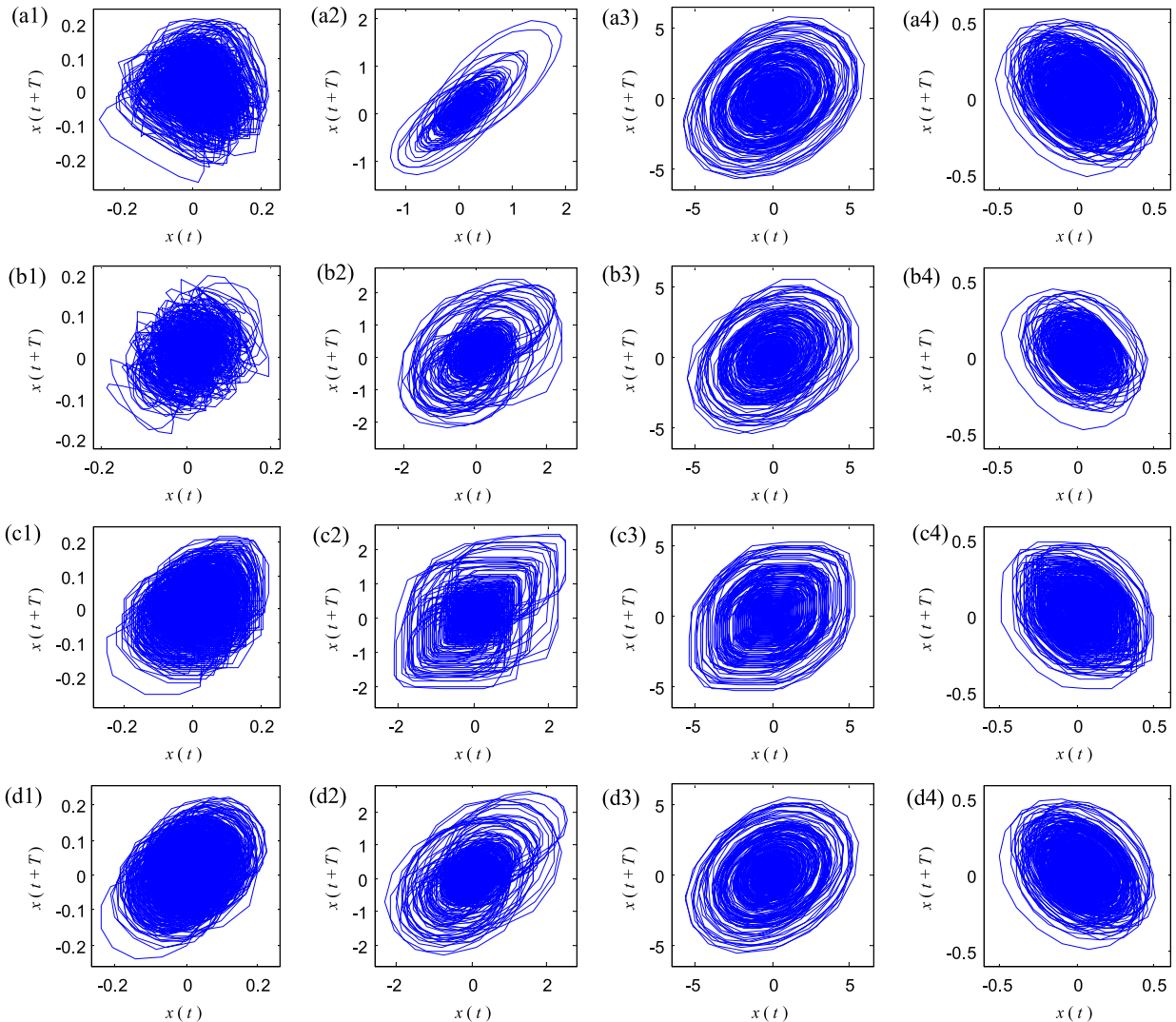

FIGURE 18. The reconstructed phase plane for denoised rolling bearing signals: (a1) -(a4) are signals denoised by EMD-CIIT, (a1) normal bearing, (a2) inner race fault, (a3) outer race fault, (a4) ball fault, (b1) -(b4) are signals denoised by WT, (b1) normal bearing, (b2) inner race fault, (b3) outer race fault, (b4) ball fault, (c1) -(c4) are signals denoised by MMF, (c1) normal bearing, (c2) inner race fault, (c3) outer race fault, (c4) ball fault, (d1) -(d4) are signals denoised by SMMF, (d1) normal bearing, (d2) inner race fault, (d3) outer race fault, (d4) ball fault.

0.011 in. (0.279 mm) depth defect single-point fault on the inner race, the outer race, the ball, and normal bearing were adopted in the experiment. The bearing geometry is shown in Table 8.

The dynamometer is used to measure the load of motor, and the transducer/encoder is capable to record rotational speed. In the experiment, the load of 0 hp is utilized to verify the effectiveness of the mentioned method. The shaft
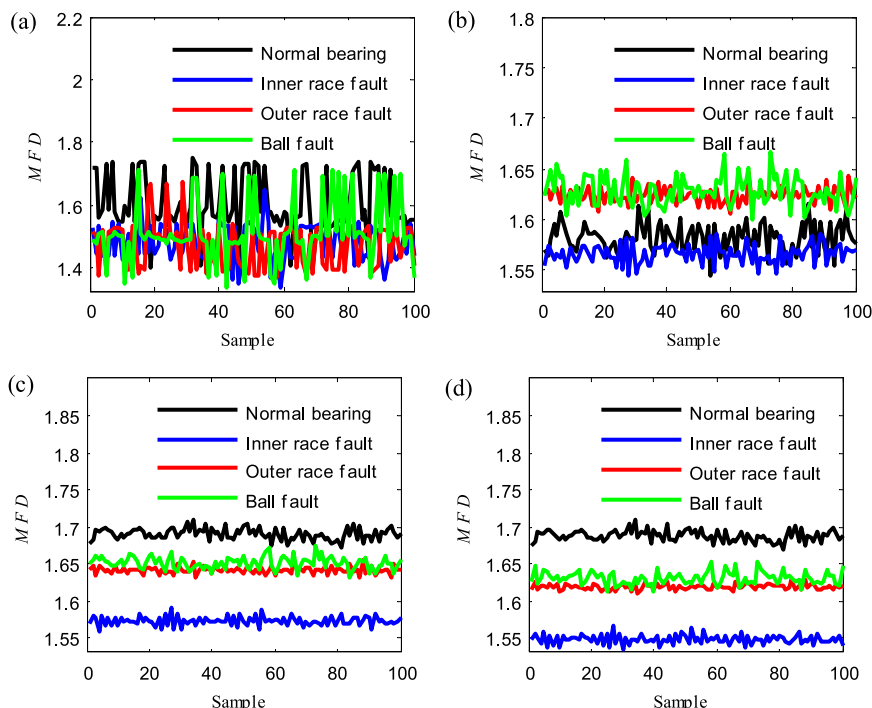
FIGURE 19. The MFD denoised bearing signals: (a) EMD-CIIT denoised signals, (b) WT denoised signals, (c) MMF denoised signals, (d) SMMF denoised signals.

TABLE 8. Parameters of experimental bearing.

Roller diameter	Pitch diameter	Number of balls	Contact angle
8.18 mm	38.5 mm	9	0°

rotation speed is 1797 rpm, the vibration data of healthy and faulty bearing were collected at 12000 Hz and 48000 Hz, respectively. Fig. 16 shows the time-domain waveform of the first 6000 points data collected in four conditions.

Fig. 18 (a1) -(a4) shows the denoised results by EMD-CIIT, as seen in figures, there is no obvious change in the reconstructed phase diagram of normal bearing signals, outer race fault signals, and ball fault signals, while the attractor of inner race fault signal has a significant change. Phase trajectories of denoising results by WT are plotted in Fig. 18 (b1) -(b4). After noise reduction, the projection of all signals changes, but the trajectories of attractors are not smooth and clear. The phase diagrams for the MMF denoising signals are shown in Fig. 18 (c1) -(c4), the trajectories of attractors reconstructed by the four types of signals are clear but not smooth. The projection of phase trajectories for SMMF denoising signals are shown in Fig. 18 (d1) -(d4). It is clear to see that the orbits of the attractor obtained by SMMF technology are more regular than the orbits obtained by other denoising technologies. It was also observed that the orbits are the smoothest of all denoised normal bearing vibration signals.

The MFD and CMMFD extracted by four methods are employed as feature vectors for distinguishing bearing states, they are applied as input to train the HMM classifier, then the feature set is distinguished. Table 9 lists the fault classification results of each feature vector as the input of HMM. It can be seen from Table 9. Most samples are given the right classify results by using different feature extracting techniques. Compared with the same feature extracted from different denoising techniques, SMMF achieves the highest accuracy. And CMMFD achieves better distinguish results by comparing the MFD feature and CMMFD feature extracted from the same signal.

TABLE 9. Fault identification results.

Algorithms	Normal bearing (%)	Inner race fault (%)	Outer race fault (%)	Ball bearing fault (%)
EMD -MFD	89	77	73	67
WT -MFD	100	72	85	69
MMF-MFD	100	50	88	77
SMMF -MFD	100	98	100	89
EMD -CMMFD	98	85	91	92
WT -CMMFD	100	91	95	88
MMF-CMMFD	100	99	90	98
SMMF -CMMFD	100	100	100	100

The results of the above simulation and experiments verified that the proposed SMMF can effectively reduce the noise. For the original signal with fuzzy attractor, SMMF is able to suppress the noise hidden in the chaotic signal effectively. For the original signal with clear attractor, SMMF is able to
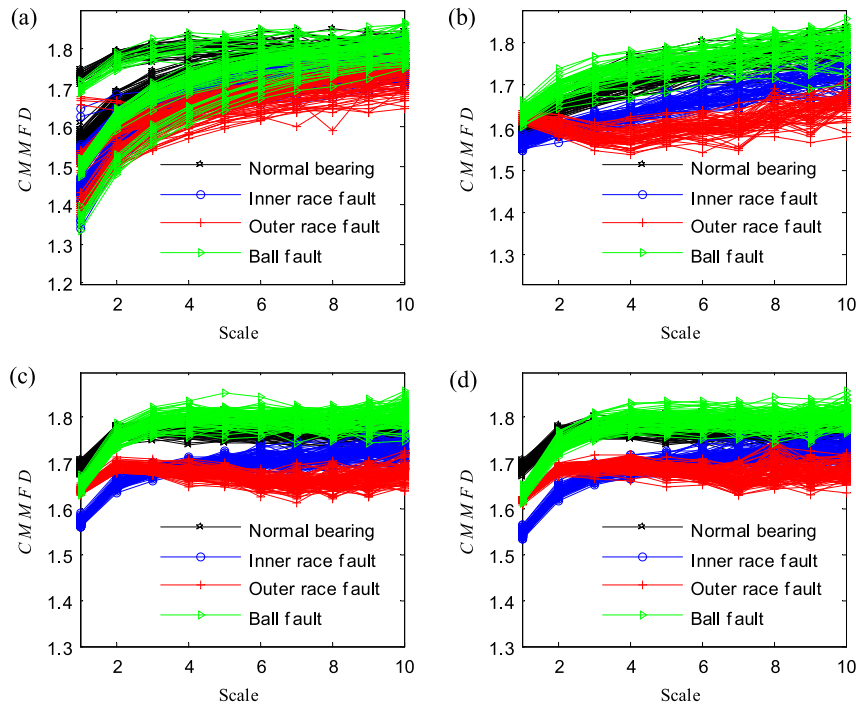
FIGURE 20. The CMMFD denoised bearing signals: (a) EMD-CIIT denoised signals, (b) WT denoised signals, (c) MMF denoised signals, (d) SMMF denoised signals.

smooth the orbits without destroying the dynamic of rolling bearing signals. And CMMFD feature based on chaotic dynamic can reflect the change of dynamic rolling bearing system sensitively. The effectiveness of SMMF-CMMFD to distinguish the normal/faulty rolling bearing is verified.

VII. CONCLUSION

In this paper, we propose a novel feature extraction method based on SMMF and CMMFD for fault detection and identi-fication in rolling bearing signals. Firstly, to suppress noise without destroying the dynamics of rolling bearing sig-nals, the modified method called SMMF which adopts the B-Spline to smooth the MMF is introduced to denoise the rolling bearing vibration signals. Afterward, a new set of features referred to as CMMFD is proposed for quantifying the change in dynamics behavior of ball bearing vibration signals. By using SMMF and CMMFD, a novel fractal feature space is constructed, and different types of fault bearing signals are distinguished from each other. To evaluate the proposed method. Fractal features space is input into a HMM classifier for detection and classification of rolling bearing signals. The results of simulation and experiment demon-strated that the proposed method is capable in extraction of fractal characteristics and identification of the type of rolling bearing signals. The ability of SMMF method to suppress noise without damaging nonlinear dynamics of rolling rear-ing signals is satisfactory, better than the EMD-CIIT, WT, and MMF. The CMMFD feature contains a wealth of information from rolling bearing vibration signals, which improves the

classification ability of MFD. In the future, we will further explore the application of this method in mixed fault types of identification and the performance degradation assessment of bearings.

REFERENCES

[1] R. Rubini and U. Meneghetti, "Application of the envelope and wavelet transform analyses for the diagnosis of incipient faults in ball bearings," *Mech. Syst. Signal Process.*, vol. 15, no. 2, pp. 287–302, Mar. 2001.

[2] Z. Huo, Y. Zhang, G. Jombo, and L. Shu, "Adaptive multiscale weighted permutation entropy for rolling bearing fault diagnosis," *IEEE Access*, vol. 8, pp. 87529–87540, 2020.

[3] C. Zhang and Y. Liu, "A two-step denoising strategy for early-stage fault diagnosis of rolling bearings," *IEEE Trans. Instrum. Meas.*, vol. 69, no. 9, pp. 6250–6261, Sep. 2020.

[4] Z. Huo, Y. Zhang, L. Shu, and M. Gallimore, "A new bearing fault diagnosis method based on fine-to-coarse multiscale permutation entropy, Laplacian score and SVM," *IEEE Access*, vol. 7, pp. 17050–17066, 2019.

[5] A. Glowacz, W. Glowacz, Z. Glowacz, and J. Kozik, "Early fault diagnosis of bearing and stator faults of the single-phase induction motor using acoustic signals," *Measurement*, vol. 113, pp. 1–9, Jan. 2018.

[6] S. Qian and D. Chen, "Decomposition of the Wigner–Ville distribution and time-frequency distribution series," *IEEE Trans. Signal Process.*, vol. 42, no. 10, pp. 2836–2842, Oct. 1994.

[7] W. Sun, G. An Yang, Q. Chen, A. Palazoglu, and K. Feng, "Fault diagnosis of rolling bearing based on wavelet transform and envelope spectrum correlation," *J. Vib. Control*, vol. 19, no. 6, pp. 924–941, Apr. 2013.

[8] Y. Lei, J. Lin, Z. He, and M. J. Zuo, "A review on empirical mode decom-position in fault diagnosis of rotating machinery," *Mech. Syst. Signal Process.*, vol. 35, nos. 1–2, pp. 108–126, Feb. 2013.

[9] K. Dragomiretskiy and D. Zosso, "Variational mode decomposition," *IEEE Trans. Signal Process.*, vol. 62, no. 3, pp. 531–544, Feb. 2014.

[10] A. Soleimani and S. E. Khadem, "Early fault detection of rotating machin-ery through chaotic vibration feature extraction of experimental data sets," *Chaos, Solitons Fractals*, vol. 78, pp. 61–75, Sep. 2015.

[11] X. Han and X. Chang, "An intelligent noise reduction method for chaotic signals based on genetic algorithms and lifting wavelet transforms," *Inf. Sci.*, vol. 218, pp. 103–118, Jan. 2013.

[12] L. Shang and K. Shyu, "A method for extracting chaotic signal from noisy environment," *Chaos, Solitons Fractals*, vol. 42, pp. 1120–1125, Oct. 2009.

[13] M. Han, Y. Liu, J. Xi, and W. Guo, "Noise smoothing for nonlinear time series using wavelet soft threshold," *IEEE Signal Process. Lett.*, vol. 14, no. 1, pp. 62–65, Jan. 2007.

[14] Y. Chen, X. Liu, Z. Wu, Y. Fan, Z. Ren, and J. Feng, "Denoising of contaminated chaotic signals based on collaborative filtering," *Acta Phys. Sinica*, vol. 66, Nov. 2017, Art. no. 210501.

[15] J. Serra and L. Vincent, "An overview of morphological filtering," *Circuits Syst. Signal Process.*, vol. 11, no. 1, pp. 47–108, Mar. 1992.

[16] J. Wang, G. Xu, Q. Zhang, and L. Liang, "Application of improved morphological filter to the extraction of impulsive attenuation signals," *Mech. Syst. Signal Process.*, vol. 23, no. 1, pp. 236–245, Jan. 2009.

[17] C. Li and M. Liang, "Continuous-scale mathematical morphology-based optimal scale band demodulation of impulsive feature for bearing defect diagnosis," *J. Sound Vib.*, vol. 331, no. 26, pp. 5864–5879, Dec. 2012.

[18] S. Mukhopadhyay and B. Chanda, "A multiscale morphological approach to local contrast enhancement," *Signal Process.*, vol. 80, no. 4, pp. 685–696, Apr. 2000.

[19] L. Zhang, J. Xu, J. Yang, D. Yang, and D. Wang, "Multiscale morphology analysis and its application to fault diagnosis," *Mech. Syst. Signal Process.*, vol. 22, no. 3, pp. 597–610, Apr. 2008.

[20] Y. Dong, M. Liao, X. Zhang, and F. Wang, "Faults diagnosis of rolling element bearings based on modified morphological method," *Mech. Syst. Signal Process.*, vol. 25, pp. 1276–1286, May 2011.

[21] A. S. Raj and N. Murali, "Early classification of bearing faults using morphological operators and fuzzy inference," *IEEE Trans. Ind. Electron.*, vol. 60, no. 2, pp. 567–574, Feb. 2013.

[22] Y. Li, M. J. Zuo, J. Lin, and J. Liu, "Fault detection method for railway wheel flat using an adaptive multiscale morphological filter," *Mech. Syst. Signal Process.*, vol. 84, pp. 642–658, Feb. 2017.

[23] C. Shen, Q. He, F. Kong, and P. W. Tse, "A fast and adaptive varying-scale morphological analysis method for rolling element bearing fault diagnosis," *Proc. Inst. Mech. Eng., C, J. Mech. Eng. Sci.*, vol. 227, no. 6, pp. 1362–1370, Jun. 2013.

[24] B. Li, P. Zhang, Z. Wang, S. Mi, and Y. Zhang, "Gear fault detection using multi-scale morphological filters," *Measurement*, vol. 44, pp. 2078–2089, Aug. 2011.

[25] P. Maragos, "Pattern spectrum and multiscale shape representation," *IEEE Trans. Pattern Anal. Mach. Intell.*, vol. 11, no. 7, pp. 701–716, Jul. 1989.

[26] P. Maragos and F.-K. Sun, "Measuring the fractal dimension of signals: Morphological covers and iterative optimization," *IEEE Trans. Signal Process.*, vol. 41, no. 1, pp. 108–121, Feb. 1993.

[27] H. Li, Y. Wang, B. Wang, J. Sun, and Y. Li, "The application of a general mathematical morphological particle as a novel indicator for the performance degradation assessment of a bearing," *Mech. Syst. Signal Process.*, vol. 82, pp. 490–502, Jan. 2017.

[28] H. Zhao, R. Yao, L. Xu, Y. Yuan, G. Li, and W. Deng, "Study on a novel fault damage degree identification method using high-order differential mathematical morphology gradient spectrum entropy," *Entropy*, vol. 20, no. 9, p. 682, Sep. 2018.

[29] B. Li, P.-L. Zhang, Z.-J. Wang, S.-S. Mi, and P.-Y. Liu, "Morphological covering based generalized dimension for gear fault diagnosis," *Nonlinear Dyn.*, vol. 67, no. 4, pp. 2561–2571, Mar. 2012.

[30] B. Wang, X. Hu, and H. Li, "Rolling bearing performance degradation condition recognition based on mathematical morphological fractal dimension and fuzzy C-means," *Measurement*, vol. 109, pp. 1–8, Oct. 2017.

[31] G. Tang, X. Yan, and X. Wang, "Chaotic signal denoising based on adaptive smoothing multiscale morphological filtering," *Complexity*, vol. 2020, pp. 1–14, Feb. 2020.

[32] G. Zhao, Q. Liang, and T. S. Durrani, "UWB radar target detection based on hidden Markov models," *IEEE Access*, vol. 6, pp. 28702–28711, May 2018.

[33] Y. Li, L. Cui, and C. Lin, "Modeling and analysis for multi-state systems with discrete-time Markov regime-switching," *Rel. Eng. Syst. Saf.*, vol. 166, pp. 41–49, Oct. 2017.

[34] J. Li, X. Zhang, X. Zhou, and L. Lu, "Reliability assessment of wind turbine bearing based on the degradation-hidden-Markov model," *Renew. Energy*, vol. 132, pp. 1076–1087, Mar. 2019.

[35] X. Yan, Y. Liu, and M. Jia, "A feature selection framework-based multiscale morphological analysis algorithm for fault diagnosis of rolling element bearing," *IEEE Access*, vol. 7, pp. 123436–123452, 2019.

[36] C. Li, M. Liang, Y. Zhang, and S. Hou, "Multi-scale autocorrelation via morphological wavelet slices for rolling element bearing fault diagnosis," *Mech. Syst. Signal Process.*, vol. 31, pp. 428–446, Aug. 2012.

[37] J. Wang, L. Cui, and Y. Xu, "Quantitative and localization fault diagnosis method of rolling bearing based on quantitative mapping model," *Entropy*, vol. 20, no. 7, p. 510, Jul. 2018.

[38] Z. Hu, C. Wang, J. Zhu, X. Liu, and F. Kong, "Bearing fault diagnosis based on an improved morphological filter," *Measurement*, vol. 80, pp. 163–178, Feb. 2016.

[39] P. Maragos and R. Schafer, "Morphological filters—Part I: Their set-theoretic analysis and relations to linear shift-invariant filters," *IEEE Trans. Acoust., Speech, Signal Process.*, vol. ASSP-35, no. 8, pp. 1153–1169, Aug. 1987.

[40] P. Maragos and R. Schafer, "Morphological filters—Part II: Their relations to median, order-statistic, and stack filters," *IEEE Trans. Acoust., Speech, Signal Process.*, vol. ASSP-35, no. 8, pp. 1170–1184, Aug. 1987.

[41] C.-W. Chen and M. Li, "Improved hydrodynamic analysis of 3-D hydrofoil and marine propeller using the potential panel method based on B-spline scheme," *Symmetry*, vol. 11, no. 2, p. 196, Feb. 2019.

[42] C.-U. Choe, K. Höhne, H. Benner, and Y. S. Kivshar, "Chaos suppression in the parametrically driven lorenz system," *Phys. Rev. E, Stat. Phys. Plasmas Fluids Relat. Interdiscip. Top.*, vol. 72, no. 3, Sep. 2005, Art. no. 036206.

[43] J. Huang, X. Wang, D. Wang, Z. Wang, and X. Hua, "Analysis of weak fault in hydraulic system based on multi-scale permutation entropy of fault-sensitive intrinsic mode function and deep belief network," *Entropy*, vol. 21, no. 4, p. 425, Apr. 2019.

[44] P. Maragos and A. Potamianos, "Fractal dimensions of speech sounds: Computation and application to automatic speech recognition," *J. Acoust. Soc. Amer.*, vol. 3, pp. 1925–1932, Apr. 1999.

[45] A. R. Backes and O. M. Bruno, "Shape classification using complex network and multi-scale fractal dimension," *Pattern Recognit. Lett.*, vol. 31, no. 1, pp. 44–51, Jan. 2010.

[46] A. Rafsanjani, S. Abbasion, A. Farshidianfar, and H. Moeenfard, "Nonlinear dynamic modeling of surface defects in rolling element bearing systems," *J. Sound Vib.*, vol. 319, nos. 3–5, pp. 1150–1174, Jan. 2009.

[47] Y. Kopsinis and S. McLaughlin, "Development of EMD-based denoising methods inspired by wavelet thresholding," *IEEE Trans. Signal Process.*, vol. 57, no. 4, pp. 1351–1362, Apr. 2009.

[48] (Jul. 20, 2012). *Case Western Reserve University Bearings Data Set.* [Online]. Available: http://csegroups.case.edu/bearingdatacenter/pages/download-data-file

• • •